Anal Bioanal Chem (2011) 399:1117–1125
DOI 10.1007/s00216-010-4446-5

ORIGINAL PAPER

Compact, cost-efficient microfluidics-based stopped-flow device

Regina Bleul · Marion Ritzi-Lehnert · Julian Höth · Nico Scharpfenecker · Ines Frese · Dominik Düchs · Sabine Brunklaus · Thomas E. Hansen-Hagge · Franz-Josef Meyer-Almes · Klaus S. Drese

Received: 14 July 2010 / Revised: 15 November 2010 / Accepted: 16 November 2010 / Published online: 30 November 2010

Abstract Stopped-flow technology is frequently used to monitor rapid (bio)chemical reactions with high temporal resolution, e.g., in dynamic investigations of enzyme reactions, protein interactions, or molecular transport mechanisms. However, conventional stopped-flow devices are often overly complex, voluminous, or costly. Moreover, excessive amounts of sample are often wasted owing to inefficient designs. To address these shortcomings, we propose a stopped-flow system based on microfluidic design principles. Our simple and cost-efficient approach offers distinct advantages over existing technology. In particular, the use of injection-molded disposable microfluidic chips minimizes required sample volumes and associated costs, simplifies handling, and prevents adverse cross-contamination effects. The cost of the system developed is reduced by an order of magnitude compared with the cost of commercial systems. The system contains a high-precision valve system for fluid control and features automated data acquisition capability with high temporal resolution. Analyses with two well-established reaction kinetics yielded a dead time of approximately 8-9 ms.

Keywords Stopped flow · Microfluidics · Low sample amounts · Short dead time

R. Bleul · M. Ritzi-Lehnert (✉) · J. Höth · N. Scharpfenecker · I. Frese · D. Düchs · S. Brunklaus · T. E. Hansen-Hagge · K. S. Drese
Institut für Mikrotechnik Mainz GmbH (IMM),
Carl-Zeiss-Str. 18-20,
55129 Mainz, Germany
e-mail: ritzi@imm-mainz.de

R. Bleul · F.-J. Meyer-Almes
Hochschule Darmstadt,
Schnittspahnstr. 12,
64287 Darmstadt, Germany

Introduction

First introduced in 1940 by Chance [1] and improved in 1964 by Gibson [2], stopped-flow technology is a highly versatile and convenient method for monitoring fast reactions. It is often used to study the dynamic interactions of biomolecules or other macromolecules, where it can provide insights into the molecular details of enzyme functions, protein–protein or protein–DNA interactions, as well as molecular transport mechanisms [3–5]. Another application is in the investigation of protein folding kinetics [6]. Understanding these kinds of processes is of growing importance not only for basic research but also to the pharmaceutical industry. For example, stopped-flow technology is key in elucidating catalytic enzyme mechanisms and functions of specific proteins in an organism. Reactant concentrations can be monitored photometrically, and changes in enzyme conformation during substrate binding or product release can be tracked using fluorescent dyes. In some cases, changes in spectral properties of the reactants can be exploited to optically detect the binding process. A prerequisite, however, is that the substances be fully mixed before the onset of binding. Clearly, then, manual mixing is inadequate for observing processes on the timescale of milliseconds; a more efficient mixing method is needed [7]. Also, highly time resolved data acquisition must be available as part of the setup.

As a result of these stringent requirements, commercial stopped-flow devices have tended to be complex in design, incorporating various components (i.e., light source, amplifier electronics, detection unit, mixing station) that in the aggregate make these systems bulky, expensive to purchase and maintain, and prone to mechanical maladjustments. Typical equipment often contains two step-motor-driven syringes which push the reactants (e.g., enzyme and substrate), at very

high velocity and in one go, first through a mixing chamber and then into the optical detection cell. The detection unit, in turn, is triggered by a stop syringe. The processes within the detection cell may be monitored via changes in absorption or fluorescence intensity. Such monitoring can, however, only be initiated after the so-called dead time has elapsed, which denotes the time span between the first contact of the reactants and the beginning of measurements in the detection region which are usable for kinetics analysis. It is thus dependent on both the mixing and the transport times. In effect, only processes happening on timescales longer than the dead time can be monitored. The dead time is determined mainly by the fluid flow rate, the mixing efficiency, the volume traversed by the fluid between the mixing chamber and the detection cell, and the volume of the detection cell [8, 9].

The intricate setups of conventional stopped-flow systems necessitate relatively high sample and reagent volumes during the first operating cycle. In serial experiments conducted without changing chemicals, however, sample consumption is very low. Still, the volumes required in the first cycle are often already prohibitive as samples and reagents are expensive or hard to isolate. Volumes of up to 3 ml during setup and, subsequently, of 1 ml per experiment are not uncommon. Extensive test series probing various parameters, as are commonly performed, thus require considerable reactant quantities. Despite this high rate of sample consumption, however, most of the volume is consumed rather wastefully in the flushing and washing steps. Here is where our microfluidics-based stopped-flow system provides substantial improvements in simplicity and cost-efficiency: the use of injection-molded disposable microfluidic chips reduces the required sample volume to 20 μl even in the first experiment as flushing is no longer necessary; sample costs are hence lowered significantly; handling is simplified; and adverse cross-contamination effects are prevented.

The chip layout and material choice allow for the use of narrow-bandwidth light-emitting diodes (LED) as light sources in the UV–vis spectrum instead of conventionally used xenon and mercury arc lamps. These UV and visible LEDs can easily be replaced with ones covering different wavelengths as the case may demand, thus broadening the applicability of our approach. Furthermore, UV–vis-sensitized photodiodes covering a wide range of wavelengths are employed instead of photomultipliers for detection.

In our case, a uniform illumination of the flow channel over a length of 10 mm is achieved with integrated on-chip mirrors that reflect light toward the detection cell and the detector. Coupling the photodiode with simple but effective amplifier electronics offers excellent sensitivity and resolution over the spectral range relevant in most biological applications (i.e., 250-1,000 nm).

The overall cost of the stopped-flow device at current component prices, including costs for housing, electronics, and optical elements, is in the low four-digit euro range, which is roughly an order of magnitude lower than that of commercially available solutions. Moreover, economies-of-scale effects are expected to further lower the per-unit cost at higher production volumes.

The performance is studied using two chemical reactions as test cases:

1. Reaction I: the reduction of 2,6-dichlorophenolindophenol (DCIP) by ascorbic acid according to Tonomura et al. [8]
2. Reaction II: the fluorescence quenching of *N*-acetyltryptophanamide (NATA) by *N*-bromosuccinimide (NBS) according to Peterman [9]

The functionality of our system is evaluated by reaction III: labeling histone deacetylase like amidohydrolase (HDAH) from *Bordetella* with fluorescent dyes [19]. This bacterial amidohydrolase is structurally highly homologous to, and thus serves as an easily produced proxy for, the human histone deacetylases currently under investigation as possible targets for cancer therapy. Because of this high homology, the transferability of drug screening results is expected in many cases.

Materials and methods

Polymer chips

Poly(methyl methacrylate) (PMMA; Plexiglas® 7N) was chosen as the polymer chip material owing to its high degree of transparency in the UV range and low autofluorescence, which allows dynamic protein investigations at a wavelength of 280 nm (the intrinsic fluorescence wavelength of tryptophan).[1] Structures for fluid transport and mirrors for light reflection were machined into injection-molded chip blanks by precision milling and laser ablation technologies. The outer chip dimensions are 43 mm×64 mm. The channels for reactant inlets are 1 mm×1 mm, having a semicircular shape at the bottom (radius 0.5 mm). The T junction has a depth of 0.4 mm and a width of 0.5 mm. The length of the tapered channel is 9.5 mm and the diameter at the connection of the detection cell is 1 mm. The detection cell is 10 mm long and 1 mm in diameter. The volume of the complete structure is 64.5 μl, where the volume from the T junction to the end of the detection cell is 16.5 μl (Figs. 2, 3). The structured chip is bonded with microencapsulated foil (40 μm, polyolefin, HJ Bioanalytik, Mönchengladbach). To enhance the wettability of the channel surfaces and suppress unspecific adsorption processes, the surfaces were processed

[1] A PMMA 7 N layer of 2 mm blocks approximately 50% of the light at 280 nm. The optical path through the chip material has a length of 1 mm before plus 1 mm after the detection cell.

with ethylenediamine or ethanolamine as described by Stein et al. [19].

Instrument setup

For the electronics, controlled high-precision magnetic valves purpose-made for miniaturized instruments (The Lee Company, Westbrook, CT, USA) were used. They combine the advantages of a very fast response time (less than 1 ms), a small dead volume (a few microliters), and a low operating voltage (12 V). Valves resistant to pressures up to 120 psi (approximately 8 bar) are available. Since these valves are prone to contamination with small particles, it is recommended that the liquids be filtered before induction (preferably using pores with diameters of 10 μm). Syringe pumps are used to load the samples and to pump them without pulsation (cetoni, Korbußen/Gera, Germany).

The detection unit consists of a LED for excitation (Roithner Lasertechnik, Vienna, Austria) and photodiodes for absorption and fluorescence detection (Silicon Sensor, Berlin, Germany). The photodiodes are equipped with a cutoff or band-pass interference filter for wavelength selection. Alternatively, absorbing filters made of a bulk polymer such as polycarbonate (Makrolon® UV 2099, 2 mm, Röhm, Darmstadt, Germany) or polystyrene (1 mm, Greiner Bio-One, Solingen, Germany) could be used to separate the excitation light from the fluorescence signal if their peak wavelengths are sufficiently distant from each other (e.g., deep-UV excitation at 280 nm with UV fluorescence at 335 nm, or UV excitation at 385 nm and visible fluorescence at 480 nm).

The beam propagation inside the chip prevents direct exposure of the fluorescence detector to the excitation beam. Since the photoelectric current of the diodes is in the picoampere to microampere range, a transimpedance amplifier (sglux SolGel Technologies, Berlin, Germany) is used for signal enhancement and to transform current signals to voltage signals, the latter with amplification factors of 10^7 V/A (off-line) or 10^{10} V/A (in-line) and output signals not exceeding ±4 V. The high amplification factors used require the system to be shielded electrically with an aluminum cover, which also serves as an optical shield blocking ambient light.

The device is connected to a computer via a multifunctional data acquisition board (16-bit; National Instruments, Austin, TX, USA) providing analog input ports for data from the optical sensor and digital output ports enabling valve control in the millisecond range. The data are collected at selectable sample rates of up to 80,000 samples per second for a specified total measurement time. The instrument is controlled with LabVIEW 8.6 (National Instruments). The setup realized is shown in Fig. 1.

Figure 2 shows a schematic diagram of the microchip-based stopped-flow device. Solutions A and B are pushed into the chip using syringe pumps up to stop valve V-6, thus filling the system with liquid free of air bubbles throughout the microfluidic channel geometry. After switching valves V-4 and V-5, valve V-1 is opened for a predetermined time (e.g., 20 ms) to drive both solutions into the detection cell by virtue of a gradient in air pressure of 2 bar. The flow is actively stopped by simultaneously closing valves V-1 and V-6. Data acquisition starts upon pumping to monitor the complete process, and all measured data are stored for subsequent analysis. Once the measurement is complete, first valve V-6 is opened, then valve V-2, to ventilate the system. An additional valve and pump are integrated into the system so it can be washed after each experiment. To do so, wash buffer is pumped through the system from valve V-3, which has to be opened for this task.

Mixing

As mentioned already, fast mixing is a major requirement in highly time resolved measurements. Various mixers with mixing times down to the millisecond range are discussed in the literature [21–25]. Commercially available stopped-flow instruments most often contain ball mixers [26] utilizing the turbulent wake which occurs downstream from a spherical surface. Since mixing is ultimately a diffusion process on microscopic length scales, mixers generally aim to increase the contact area of the reactants to achieve faster mixing [21–25]. This is often achieved by subjecting the flow to turbulent flow conditions.

Falk and Commenge [25] recently demonstrated that the main factor determining mixing times is the pressure drop across the mixer. They further showed that the mixing time is governed by a common empirical scaling behavior with respect to the pressure drop across a wide array of mixer geometries and flow rates. The task of finding an appropriate mixer thus reduces to selecting a geometry that will produce the required pressure drop at the pertinent flow rate. Using this result, which holds in both the laminar and the turbulent flow regimes, we conclude that a basic T mixer geometry [27] suffices to obtain the required mixing performance.

Adjusting the pressure drop via variations in the spatial dimensions of the mixing section allows this mixer to easily fit into the overall layout of our system. At the junction of the T structure, the two solutions collide and merge at high velocities. The reactants are mixed by the induced vortices, and the reaction starts within the short mixing channel [28]. Upon leaving the mixing channel, the mixture is propelled directly into the optical detection cell.

A flow rate of 3.6 ml/s was determined by simulating fluid velocity fields within the chip at 2-bar overpressure using the computational fluid dynamics program Flow 3D (Flow Science, Santa Fe, NM, USA). The velocity is highest at the beginning of the mixing section, being approximately 20 m/s (Fig. 3). For aqueous solutions, the

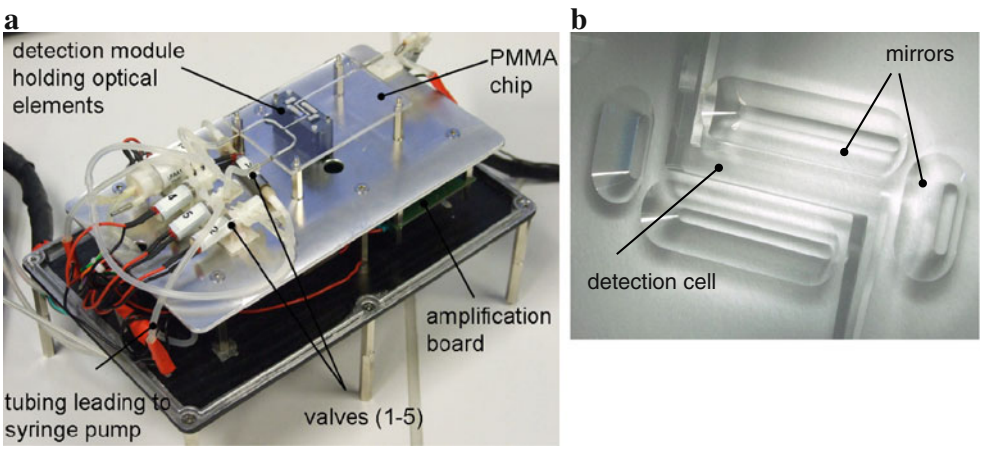

Fig. 1 **a** Laboratory setup of the microfluidic chip-based stopped-flow device [poly (methyl methacrylate) (*PMMA*) chip dimensions 64 mm× 43 mm]. **b** Close-up of detection cell with surrounding integrated 45° surfaces enabling internal reflection of excitation light (small mirrors) as well as fluorescence (larger lateral mirrors) inside the PMMA chip

calculated Reynolds number is around 9,000, indicating turbulent flow conditions (turbulence is generally found above Reynolds numbers of approximately 2,300).

Using Falk and Commenge's results, the residence time of the fluids over the T junction and the tapered section (a few milliseconds) is approximately 40% higher than the required mixing time for the geometry employed. Moreover, this ratio remains roughly constant throughout the range of typical pressures thereby ensuring satisfactory levels of mixing. Commercially available high-performance stopped-flow systems, however, offer flow rates of 13 ml/s and dead times less than 1.5 ms (Table 1).

The flow may be accelerated by increasing the applied pressure. As a result, turbulences will tend to be amplified, leading to faster mixing and shorter dead times (as defined above).

Dead time determination by absorption and fluorescence measurements—reactions I and II

The dead time of the stopped-flow device is defined as the time interval from the onset of the reaction of interest to the time when it can first be monitored. It depends mainly on the mixing time, the flow rate, and the dead volume and can be determined from signals (e.g., absorption or fluorescence) measured in simple first-order reactions [8, 9]. To examine the dead time of our device, we measured reaction I (by absorption) and reaction II (by fluorescence) as described in "Introduction." In both cases, a signal (absorption or fluorescence) is obtained which varies as the chemical reaction progresses. Although the reaction starts immediately upon first contact of the reactants, this initially happens outside the detection zone.

Moreover, to obtain reliable data, valves V-1 and V-6 are closed after the initial transport time has elapsed and the fluid volume previously present in the detection zone has been flushed out. After the fluid flow has been stopped, it still takes approximately 10 ms before data points usable for kinetics analyses are obtained (Fig. 4).

We therefore discard all data taken less than 10 ms after the simultaneous closing of valves V-1 and V-6 and shift the time axis to this point in time, denoting it by $t=0$. The resulting graphs are characterized by a quick ascent at short times followed by an equilibrium state at long times, as one would expect from a saturating

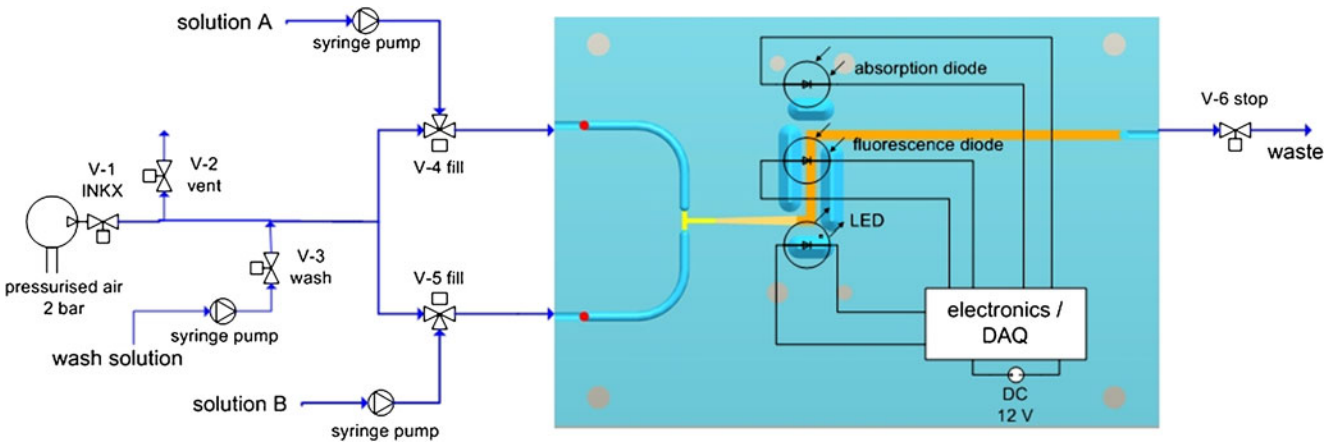

Fig. 2 The microchip-based stopped-flow device

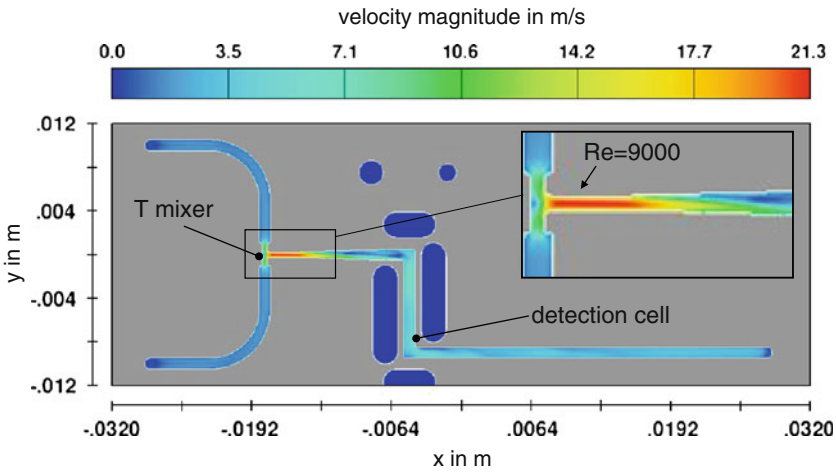

Fig. 3 Snapshot of velocity magnitude distribution of the microfluidic T mixer structure with an adjacent tapered channel and detection cell obtained by transient computational fluid dynamics simulation using Flow3D. *Dark blue* represents open regions in the chip such as mirrors and bore holes. T mixer dimensions 0.5-mm×0.4-mm channel diameter, 3-mm outlet length, 9.5-mm-long tapered channel

reaction (also see Fig. 5a). An appropriate fit for this behavior is given by Eq. 1:

$$a + bt + ce^{-kt}, \tag{1}$$

where the term bt represents the influence of drift in the measuring device. The fit parameters a, b, c, and k are calculated with the solver integrated in Microsoft Excel. For better statistics, this is not done on results from a single experiment. Rather, we run the same experiment several times and normalize the resulting data sets by multiplying them by gauge factors such that the medians of the last ten data points of each graph coincide. Then we carry out the fit on the averaged signal plot.

For each set of experiments at different reactant concentrations, we repeat the procedure just described. The rate constant, k, of the reaction is obtained for each concentration directly as part of the respective fit. To determine the dead time, we proceed as follows. First, the median-normalized and averaged signal plots for the different reactant concentrations (as shown, e.g., in Fig. 5b) are shifted relative to each other such that the endpoints of their fits coincide. The objective here is to gauge all graphs to a common asymptote representing the saturation stage of the reaction. It is pertinent that the drift parameter, b, varied only very slightly (typically less than 2%) across fits for different concentrations, justifying our normalization procedure.

The point at $t<0$ where the graphs intersect marks the lower end of the dead time interval. The upper end is given by $t=0$. Following Peterman [9], we plot the logarithm of the graphs after subtracting their long-time limits (thereby "linearizing" them; see, e.g., Fig. 5c) to better discern their common crossing point. The dead time is then given by the distance on the time axis between this point and $t=0$.

HDAH expression, isolation, and labeling with fluorescamine–reaction III

HDAH was expressed in, and purified from, bacterial strain XL1-Blue-FB188-HDAH. The strain and protocols were kindly provided by C. Hildmann (TU Ilmenau, Ilmenau,

Table 1 Dead times of commercial systems

Company/product	Dead time (ms)	Reference
Applied Photophysics SX 18MV	≈2	[10]
Applied Photophysics SX MV	2 (Fluo), 8 (CD)	[11]
Applied Photophysics SPF-17	15	[12]
AVIV Instruments stopped-flow tower interface with AVIV 202 SF spectrometer	5	[13]
BioLogic SFM-4	15	[14]
BioLogic SFM-20	<1.5	[15]
TgK Scientific HPSF-56	<10	[16]
Unisoku RSP-1000 (Japan)	3	[17]
Unisoku type USP-539	15	[18]

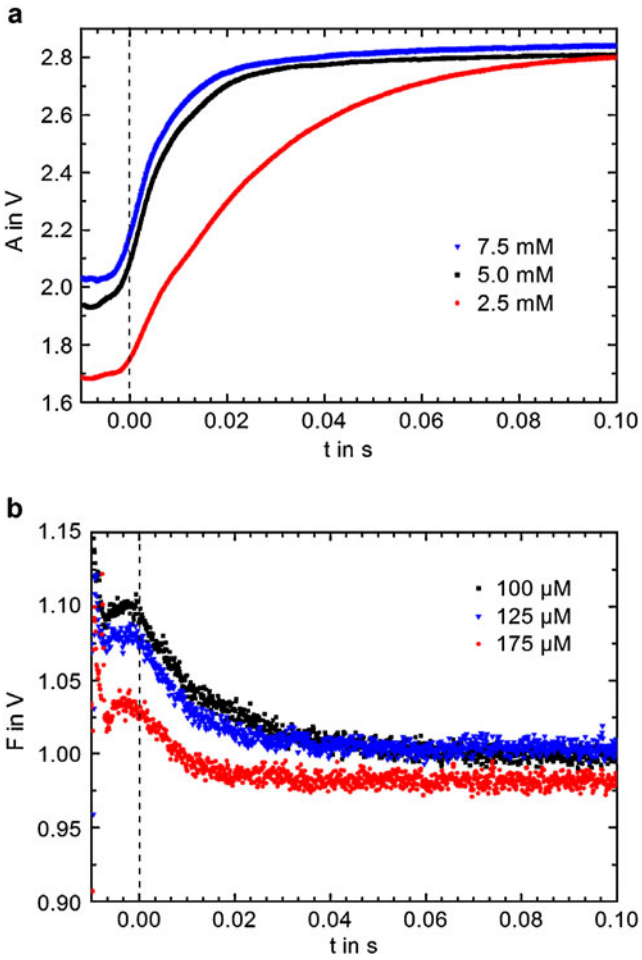

Fig. 4 Signals recorded after closing the valves: **a** absorption in reaction I at several ascorbic acid concentrations, and **b** fluorescence intensity in reaction II at several *N*-bromosuccinimide (NBS) concentrations. The time axis is shifted to the start of the first usable data for kinetics analysis (t=0, *dashed line*)

Germany). The HDAH concentration was determined using a bicinchoninic acid protein determination kit (Interchim) as prescribed by the manufacturer. When excited at 390 nm, fluorescamine (4-phenylspiro-[furan-2(3*H*),1-phthalane]-3,3′-dione) exhibits strong fluorescence at 475-490 nm when bound to proteins. For the reaction of 3 μM HDAH in 0.2 M borate, a buffer with a pH of 8.6 was mixed 1:1 with 1-4 mM fluorescamine in dimethyl sulfoxide. For optical detection, a 385-nm LED was used. The amplifier gain was set to $5 \cdot 10^7$ V/A.

The data from reaction III were fitted to the expression $a + bt + c \exp(-kt)$ in the same fashion as for reactions I and II to obtain reaction rate constants, k. Since the dead time is not a critical parameter for this analysis, it was not determined again here. The signal plots used (Fig. 7) show clearly undisturbed data, justifying our analysis procedure.

Results and discussion

Dead time determination by absorption measurements—reaction I

The first reaction used to determine the dead time of the system was the reduction of DCIP by ascorbic acid (Fig. 5). Data were acquired at a sample rate of 10,000 s^{-1} (individual measurements, no integration was performed) starting 10 ms after the closing of stop valve V-6. Analyses of seven independent measurements revealed an average rate constant, k, of $(94 \pm 13) s^{-1}$. After averaging and data fitting, we obtained a rate constant, k, of 91.1 s^{-1} (Fig. 5a).

The reaction speed can be influenced by varying the concentration, yielding half-lives shorter than 1 ms. For the reaction, 5-20 mM ascorbic acid in 0.2 M NaCl at pH 4 was mixed 1:1 with 140 μM DCIP. For the optical detection, a 525-nm LED and a detector with an interference filter (536 nm, band width 40 nm) were used. The amplifier gain was set to 10^9 V/A.

Repeating the same experiments with different ascorbic acid concentrations (2.5-10 mM) reveals a nearly linear dependence of the rate constant on the ascorbic acid concentration (inset in Fig. 5b). The dead time is obtained as described above and amounts to approximately 9 ms, which is competitive with conventional stopped-flow systems, e.g., from TgK Scientific (Bradford-on-Avon, UK), whose dead times are specified as 8-10 ms.

Rate constants for the DCIP reduction by ascorbic acid, however, are difficult to compare since for pH 4 Tonomura et al. [8] only reported data for a higher ascorbic acid concentration (20 mM). Moreover, between pH 4 and pH 5, the rate constants are rather sensitive to the pH of the reaction mixture (pH 4.07, k=838 s^{-1}; pH 4.91, k=224 s^{-1} [8]). Yet, the rate constant of 149 s^{-1} (Fig. 5) determined with our stopped-flow device for 10 mM ascorbic acid lies in the anticipated range, since a linear extrapolation of pH-dependent data given in [8] to lower concentrations results in k values of 419 and 112 s^{-1} for pH 4.07 and pH 4.91, respectively.

Dead time determination by fluorescence measurements–reaction II

Another standard reaction for the determination of the dead time is the pseudo-first-order quenching reaction of NATA by NBS, which exhibits rate constants, k, ranging from 70 to 155 s^{-1} [9]. Experiments were conducted using 10 μM NATA (Sigma-Aldrich) mixed 1:1 with 200-400 μM NBS (Sigma-Aldrich), leading to total NBS concentrations of 100-200 μM. The excitation wavelength was 280 nm, and the emission was measured above 300 nm using a polystyrene filter. All

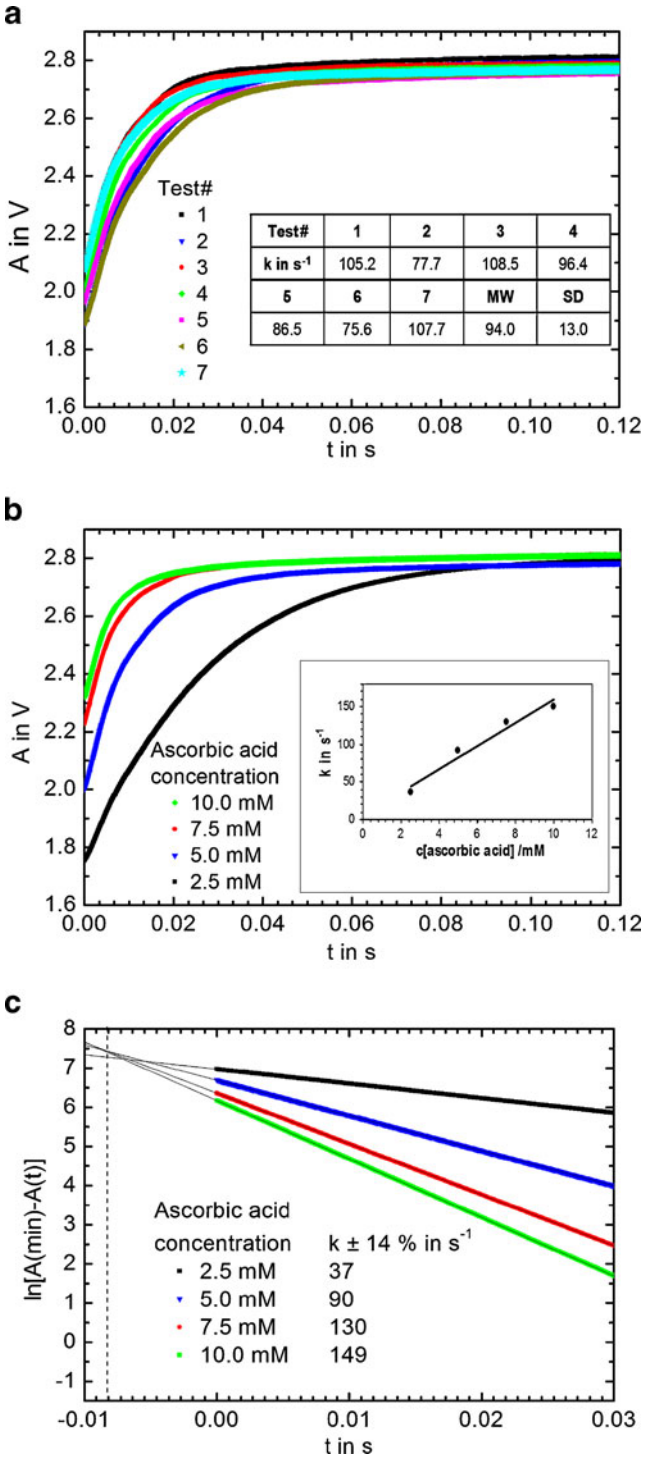

Fig. 5 Reduction of 2,6-dichlorophenolindophenol (DICP) by ascorbic acid. **a** Individual absorption measurements with 70 μM DCIP+5 mM ascorbic acid, pH 4, 22 °C. **b** Average of seven independent measurements for each ascorbic acid concentration (70 μM DCIP). The *inset* shows the linear dependence (R^2=0.9611) of the rate constant, *k*, on ascorbic acid concentration, *c*. **c** Dead time plot of linearized curves from **b**. The resulting dead time is approximately 9 ms (*dashed line*)

solutions were freshly made in degassed 50 mM phosphate buffer, with a pH of 7 in a nitrogen atmosphere. For the optical detection, the LED was combined with a polystyrene absorption filter. Being able to conduct measurements in the UV range is of particular interest in investigations involving the intrinsic fluorescence present in proteins.

An analysis of four independent measurements for each NBS concentration is shown in Fig. 6. It can be seen that the data are approximated well by exponentials (the drift parameters, *b*, are within a few percent of each other and so can be neglected in evaluating the dead time, as per the earlier discussion). A dead time plot was obtained in the same fashion as for the absorption experiments, again yielding a dead time estimate of approximately 8 ms and thus corroborating the earlier result. The first-order rate coefficient, *k*, determined for the quenching of NATA

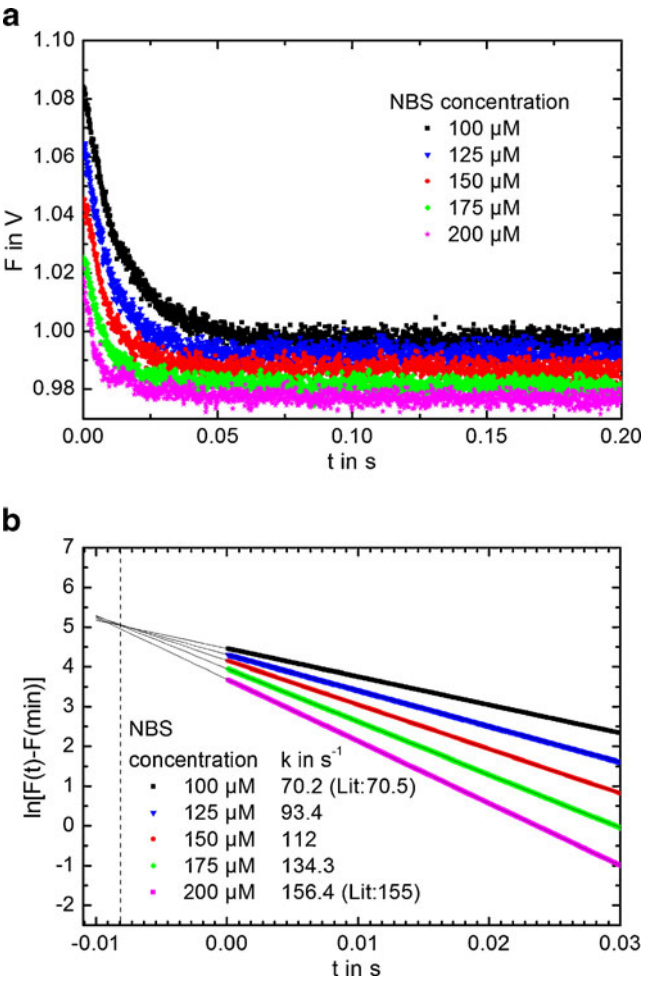

Fig. 6 Quenching of *N*-acetyltryptophanamide (NATA; 5 μM) by NBS, pH 7, 23 °C: **a** Average of four independent measurements of fluorescence intensity, *F*, for each NBS concentration. **b** Determination of dead time (*dashed line* at *t*=–8 ms) and first-order rate coefficient, *k*, for the quenching of NATA fluorescence by NBS with the present stopped-flow system in comparison with published data [9]

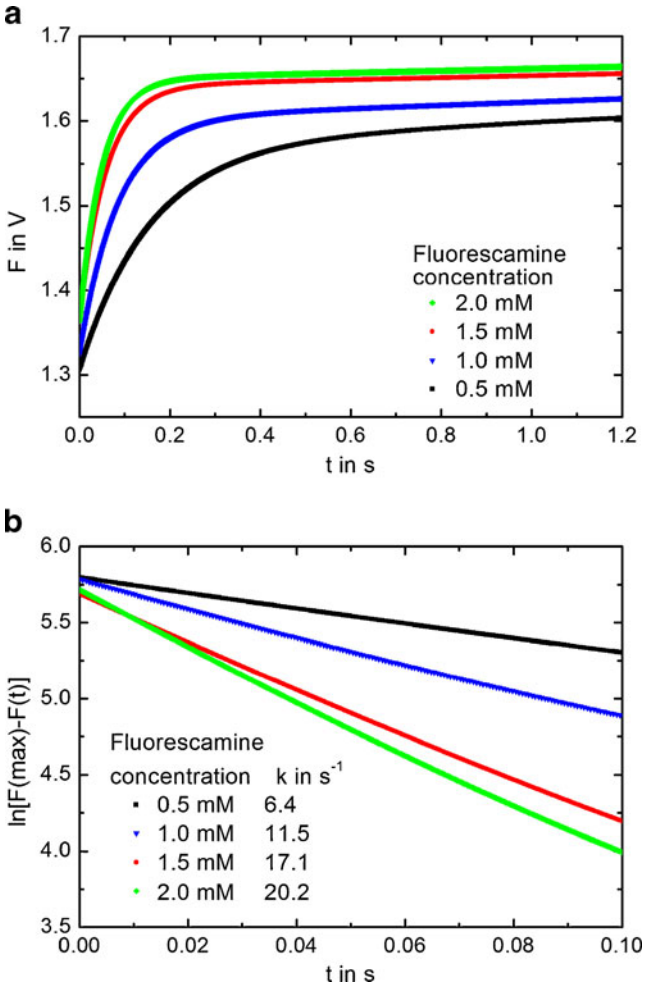

Fig. 7 Labeling of histone deacetylase like amidohydrolase (HDAH) with fluorescamine. **a** Fluorescence intensity measured for 3 μM HDAH mixed 1:1 with fluorescamine in dimethyl sulfoxide at 22 °C; average of four independent measurements for each fluorescamine concentration. **b** Natural logarithm of the difference of the maximum observed fluorescence intensity and time-dependent intensity, plotted against time. The values determined for k are shown

fluorescence by NBS with the present stopped-flow system is comparable to published data [9].

Functionality evaluation using HDAH–reaction III

Since the system seemed capable of determining reaction kinetics reproducibly and in accordance with published data, additional experiments were done to evaluate its functionality. As a test case for a two-step reaction, labeling of HDAH with fluorescamine was examined, where the following mechanism was proposed by Stein et al.[2]:

$$\mathrm{F} + \mathrm{A} \underset{k_{-1}}{\overset{k_1}{\rightleftharpoons}} [\mathrm{F}\cdot\mathrm{A}] \xrightarrow{k_2} \mathrm{P}. \tag{2}$$

[2] The reaction was set up following a protocol described in [19] for the labeling of alanine.

F represents fluorescamine, A stands for HDAC, [F·A] denotes an intermediate complex, and P is the fluorescent labeled product. From the experimental results shown in Fig. 7, an apparent pseudo-first-order reaction rate, k, can be determined. Following the proposed reaction mechanism, k_1/k_{-1} and k_2 are calculated utilizing the linear relation

$$\frac{1}{k} = \frac{1}{k_2} + \frac{k_{-1}}{k_1 k_2}\frac{1}{[\mathrm{F}]}. \tag{3}$$

The equilibrium constant for intermediate complex formation, k_1/k_{-1}, as obtained from Eq. 3 is 0.9 mM^{-1}, whereas in [19] a corresponding k_1/k_{-1} of 0.2 mM^{-1} was reported for a similar reaction of fluorescamine with a primary amine (alanine). The rate constant $k_2 \approx 78$ s^{-1} of the subsequent irreversible reaction step, however, is fairly comparable to $k_2 \approx 100$ s^{-1} given in [19]. Therefore, both values confirm the suitability of our stopped-flow device for analysis of two-step reaction kinetics.

Conclusion and outlook

A microchip-based automated stopped-flow device has been presented whose small size and significantly reduced reagent consumption represent an important advance for the measurement of highly time resolved reaction kinetics. The present system now puts applications previously not considered feasible, owing either to prohibitive costs or insufficient amounts of available reagent volumes, within the realm of possibility. Based on a microfluidic polymer chip and a compact custom-made instrument, the system is flexible in application, easy to handle, and cost-efficient in both acquisition and operation. The overall cost of the system presented here (low four-digit euro range) is roughly an order of magnitude lower than that of commercially available systems. Economies-of-scale effects are expected to further reduce per-unit costs and thus open up a path to providing low-cost solutions to end users.

Allowing linear absorption measurements up to about $A_{490}=1.5$ and a lower detection limit of fluorescein (excitation wavelength, 490 nm; emission wavelength 530 nm; amplification 10^7 V/A) at 50 nM, it is as efficient as most conventional photometers (the most sensitive fluorescence spectrometers have detection limits down to 5 nM fluorescein [29]). The integration of a stop valve helps make the fluid control more robust. The possibility to wash the system after each experiment allows for consecutive series of measurements on the same chip.

To validate the performance and to determine the dead time of the microchip-based stopped-flow device, three different reactions were investigated. Also, measurements in the UV range can be conducted, e.g., for investigations of the intrinsic fluorescence of proteins. Our investigations

showed agreement with data published in the literature for all three test reactions. In particular, two reactions showed dead times of approximately 8-9 ms, which is competitive with conventional stopped-flow systems. In the third reaction, kinetic parameters were reproduced consistent with the published reaction scheme.

Although our system is already competitive with commercially available stopped-flow systems, a further reduction in dead times to approximately 0.25 ms will be required to approach the performance level of today's best-performing systems. Another goal is the further reduction of sample volumes. In this pursuit, reducing the channel length before the mixing structure and behind the detection cell may prove advantageous. Therefore, we envisage the integration of fast switchable valves on the chip. Despite the turbulent flow conditions prevalent in our system, the mixing efficiency can and must be enhanced. Introducing structures to that effect should shorten mixing times, which would be desirable especially for cases of asymmetric reagent volumes. Application of higher pressures will reduce the dead time further but may come at the price of reduced reproducibility due to higher turbulence. By careful design of the mixing structure, it may be possible to reduce dead times below the 1-ms mark.

References

1. Chance B (1940) J Franklin Inst 229:455–613
2. Gibson QH, Milnes L (1964) Biochem J 91:161
3. Sykora J, Meyer-Almes FJ (2010) Biochemistry 49(7):1418–1424
4. Gabibov AG, Kochetkov SN, Sashchenko LP, Smirnov IV, Timofeev VP, Severin ES (1983) Eur J Biochem 132(2):339–344
5. Biro FN, Zhai J, Doucette CW, Hingorani MM (2010) J Vis Exp (37):1874, doi:10.3791/1874
6. Kern S, Riester D, Hildmann C, Schwienhorst A, Meyer-Almes FJ (2007) FEBS J 274(14):3578–3588
7. Nienhaus U (2005) Protein-ligand interactions – methods and applications. Humana, Totowa
8. Tonomura B, Nakatani H, Ohnishi M, Yamaguchi-Ito J, Hiromi K (1978) Anal Biochem 84:370–383
9. Peterman BF (1979) Anal Biochem 93:442–444
10. Guo M, Bhaskar B, Li H, Barrows TL, Poulos TL (2004) Proc Natl Acad Sci USA 101(16):5940–5945
11. van Dael H (2003) Protein Sci 12:609–619
12. Zhang HJ, Sheng XR, Niu WD, Pan XM, Zhou JM (1998) J Biol Chem 273:7448–7456
13. Stumps MR, Gloss LM (2008) J Mol Biol 384:1369–1383
14. Engel MFM, van Mierlo CPM, Visser AJWG (2002) J Biol Chem 277:10922–10930
15. BioLogic (2010) Bio-Logic - rapid-mixing instruments. http://www.bio-logic.info/rapid-kinetics/rmi.html. Accessed 14 Sep 2010
16. TgK Scientific (2010) High-pressure stopped-flow. http://www.hi-techsci.com/products/highpressure. Accessed 14 Sep 2010
17. Kobayashi K, Yoshioka S, Kato Y, Asano Y, Aono S (2005) J Biol Chem 280:5486–5490
18. Fan YX, Zhou JM, Kihara H, Tsou CL (1998) Protein Sci 7:2631–2641
19. Stein S, Böhlen P, Udenfriend S (1974) Arch Biochem Biophys 163:400–403
20. Brown L, Koerner T, Horton JH, Oleschuk RD (2006) Lab Chip 6:66–73
21. Hardt S, Drese KS, Hessel V, Schönfeld F (2005) Microfluid Nanofluid 1:108–118
22. Green J, Holdo AE, Khan A (2007) Int J Multiphys 1(1):1–32
23. Nguyen NT, Wu Z (2005) J Micromech Microeng 15:R1–R16
24. Hessel V, Löwe H, Schönfeld F (2005) Chem Eng Sci 60:2479–2501
25. Falk L, Commenge JM (2010) Chem Eng Sci 65:405–411
26. Berger RL, Balko B, Chapman HF (1968) Rev Sci Instrum 39:493–498
27. Mansur EA, Mingxing YE, Yundong W, Youyuan D (2008) Chin J Chem Eng 16(4):503–516
28. Bothe D, Stemich C, Warnecke HJ (2006) Chem Eng Sci 61:2950–2958
29. Reynisson E, Josefsen MH, Krause M, Hoorfar J (2006) J Microbiol Methods 66(2):206–216